Supporting Information for:

Electronic Structure of a Cu^{II}-Alkoxide Complex Modeling Intermediates in Copper-Catalyzed Alcohol Oxidations

Ellen C. Hayes, Thomas R. Porter[†], Charles J. Barrows, Werner Kaminsky, James M. Mayer[‡], Stefan Stoll[*]

Department of Chemistry, Box 351700, University of Washington, Seattle, WA 98195

Present Addresses:

[†] Laboratoire d'Electrochimie Moléculaire, Université Paris Diderot, 15 Rue Jean-Antoine de Baïf, F-75205 Paris Cedex 13, France.

[‡] Department of Chemistry, Yale University, New Haven, CT.

Table of Contents

Section 1: Simulation parameters for EPR and ENDOR spectra

1.a: Simulation parameters for field swept spectra

Table S1A: Simulation parameters for field sweep frozen solution spectra in Figure 1A,B

	Principal *g* values (error)[a], gStrain	Principal ^{Cu}A values in MHz (error)[b], AStrain	Gaussian, Lorentzian peak-to-peak broadening in mT
9.22 GHz (X-band)	2.06 (0.01), 0.046 2.09 (0.01), 0.022 2.44 (0.01), 0.012	30 (29), 1 92 (20), 5 120 (10), 6	0, 1.8
34.061 GHz (Q-band)	2.060 (0.006), 0.01 2.093 (0.006), 0.02 2.447 (0.006), 0.01	30 (20), 0 92 (30), 1 118 (15) , 6	0, 1.5

[a] The error was obtained from two sources. First, we assume an error in the magnetic field measurement of 0.5 mT and 1.5 mT at X-band and Q-band, respectively. This results in *g* value errors of ≈ 0.003. Second, the simulation error was estimated by varying the individual simulation parameters until visually unsatisfactory fits of the data were obtained. These two sources of error were summed to obtain the error estimates.

[b] Simulation error is accounted for by varying the parameter until visually unsatisfactory fits were obtained.

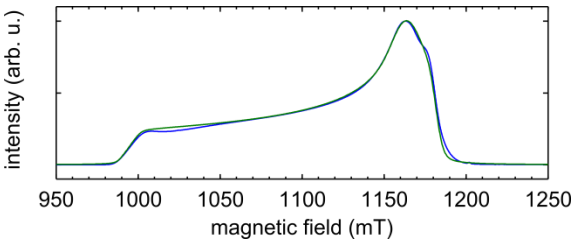

Figure S1. Pulse field swept spectrum of Cu^{II}-O(TFE) (blue) shown in Figure 2B prior to taking derivative. Simulation (green) uses the parameters from Table S1A.

Table S1B: Simulation parameters for single-crystal pulse field sweep EPR

	Principal *g* values (error)	Euler angles in degrees Molecular → *g* Frame (error)[a]	Principal ^{Cu}A values in MHz (error)[a]	Gaussian, Lorentzian peak-to-peak broadening in mT
Crystal 1 Figure 2C	2.063 (0.006) 2.093 (0.006) 2.453 (0.004)	-69 (5) -10 (3) 91 (15)	60 (30) 60 (30) 118 (10)	2, 1.5
Crystal 2 Figure S2	2.063 (0.008) 2.093 (0.02) 2.463 (0.006)	-73 (10) -10 (4) 111 (15)	60 (30) 60 (30) 118 (10)	2, 1.5

[a] Simulation error is accounted for by varying the parameter until visually unsatisfactory fits were obtained.

Table S1C: Summary of ENDOR simulation parameters for crystals 1 and 2[a]

	g values (crystal 1)	*g* values (crystal 2)	Hyperfine coupling in MHz for H_S (error)[b]	Hyperfine coupling in MHz for H_R (error)[b]
Isotropic coupling			8 (1)	25.8 (0.5)
Dipolar coupling				
xx			-3.3(0.3)	-2.5(0.2)
yy			-2.6(0.1)	-3.1(0.3)
zz			6.3(0.5)	5.5(0.5)
Principal values				
xx	2.06	2.06	4.7	23.3
yy	2.09	2.09	5.4	22.7
zz	2.45	2.46	14.3	31.3
Euler angles (degrees)	-69	-73	-73	-123
Molecular → Tensor	-10	-10	31	49
Frame	91	111	65	-31

[a] ^{1}H ENDOR simulations used identical parameters for the hyperfine coupling. However, different *g* values and molecular frame to *g* tensor frame Euler angles were used. In addition, the orientation of each crystal in the EPR spectrometer was determined by X-ray crystallography and was different for each crystal.

[b] To estimate simulation error, a range of satisfactory fits was found by simultaneously varying the spin population on oxygen (0.10 ± 0.03) and copper (0.73 ∓ 0.03). Error in the dipolar coupling was taken from the range of hyperfine coupling calculated when the spin population was varied.

1.b: Crystal 2 field swept and ENDOR data, simulations

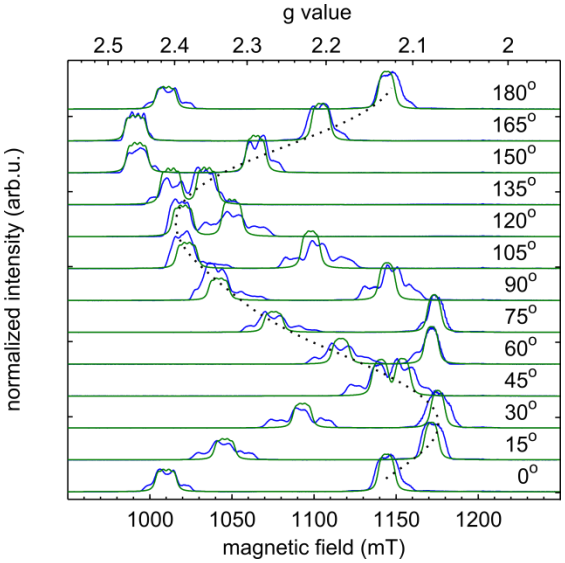

Figure S2. FID detected single-crystal spectra acquired at 34.100 GHz. Spectra were acquired at 10 K with a 1 μs π/2 pulse and 2 ms repetition time in 0.1 mT steps. Low-intensity wing features around the central transitions are due to twining of the crystal, which was confirmed by X-ray diffraction. Experimental traces are shown in blue and simulations in green. Simulation parameters are summarized in Tables S1A.

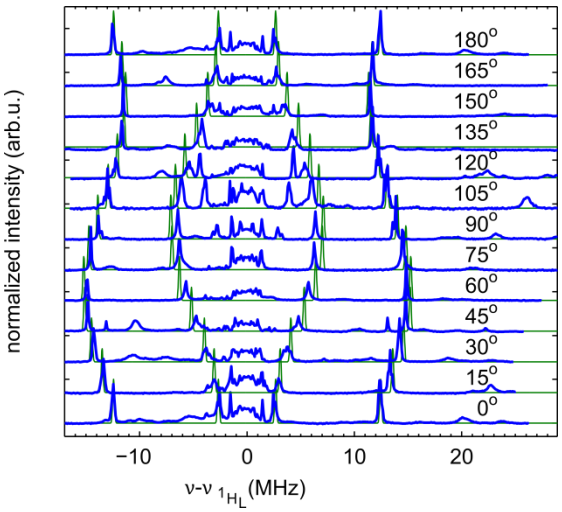

Figure S3. 34.100 GHz Davies ENDOR spectra (blue) of a single crystal of Cu^{II}-O(TFE) at 10 K. Spectra were acquired at the *g* values and magnetic fields corresponding to the site marked with a dotted line in Figure S2. π/2 and π pulse lengths were 40 ns and 80 ns with a spacing τ = 230 ns. A 13 μs RF pulse was applied. Spectra were acquired with a 3 ms repetition time with a frequency resolution of 0.1 MHz. Simulations are shown in green (simulation parameters in Table S1C).

1.c: Supplemental ENDOR spectra

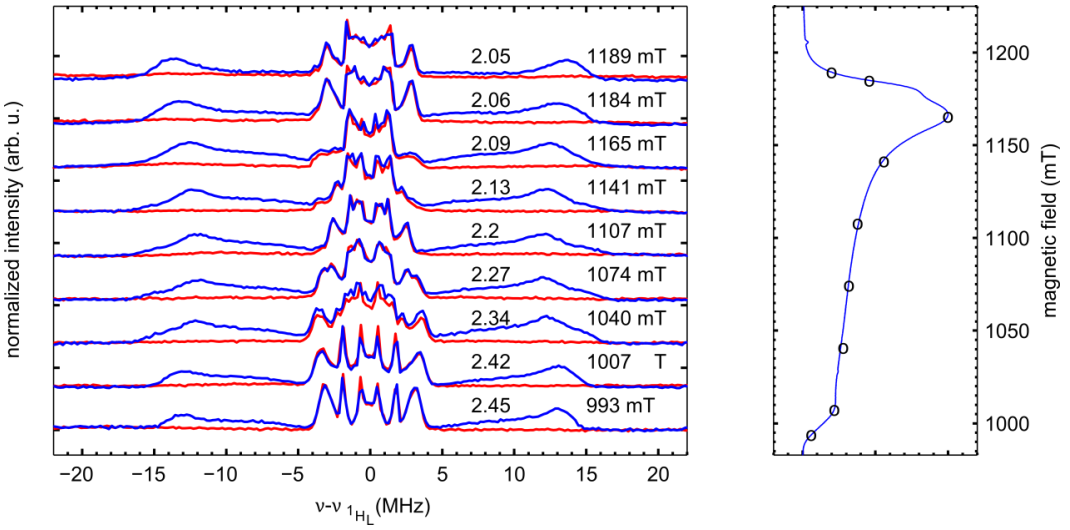

Figure S4. Davies ENDOR spectra of a frozen solution of Cu^{II}-O(TFE) at 10 K (blue, 34.118 GHz) and Cu^{II}-O(TFE)-d_2 (red, 34.068 GHz) in 1:1 DCM:toluene. Spectra were acquired at the *g* values and fields listed in the figure for the protiated sample. Due a frequency shift in the spectrometer with the deuterated sample, the fields where data were recorded were adjusted to correspond to the listed *g* values. Magnetic fields were measured with a Hall probe, the frequency was measured with the internal counter in the Bruker spectrometer. $\pi/2$ and π pulse lengths were 40 ns and 80 ns with a spacing τ = 240 ns. A 14.5 μs RF pulse was applied. Spectra were acquired with a 3 ms repetition time with a resolution of 0.2 MHz.

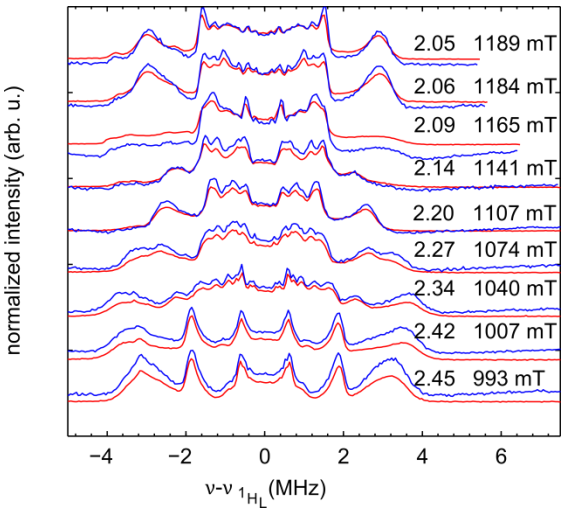

Figure S5. Davies ENDOR spectra of a frozen solution of Cu^{II}-O(TFE) (blue, 34.118 GHz) and Cu^{II}-O(TFE)-d_2 (red, 34.068 GHz) at 10 K in 1:1 DCM:toluene. Spectra of Cu^{II}-O(TFE) were acquired at the fields and *g* values listed in the figure. The fields used to calculate the listed *g* values were down shifted by 1.5 mT to account for a known deviation between the field value measured by the spectrometer Hall probe and the actual field at the sample location. Due to a frequency shift in the spectrometer for the Cu^{II} -O(TFE)-d_2 sample, the magnetic field where each spectrum was recorded was adjusted to correspond to the listed *g* values. The frequency was recorded on the internal counter in the Bruker spectrometer. $\pi/2$ and π pulse lengths were 40 ns and 80 ns with a spacing τ = 240 ns. A 14.5 μs RF pulse was applied. Spectra were acquired with a 3 ms repetition time with a resolution of 0.2 MHz.

Table S1D: Simulation parameters for ^{19}F and ^{14}N ENDOR spectra in Figure 5A, B (hyperfine coupling in MHz).

	g	F1[a]	F2[a]	F3[a]	N_{1basal}[b]	N_{2basal}[b]
Isotropic coupling		0	0	0	32.9	31.9
Dipolar coupling						
xx		-1.12(0.07)	-0.65(0.04)	-1.11(0.08)	-4.1	-1.6
yy		-1.44(0.09)	-0.75(0.04)	-1.31(0.02)	-4.1	-1.6
zz		2.37(0.2)	1.35(0.08)	2.24 (0.2)	8.2	3.2
Principal values						
xx	2.06				28.8 (8)	30.3(2)
yy	2.09				28.8 (3)	30.3(2)
zz	2.45				41.1 (1)	35.1(2)
Euler angles (degrees)	-69	-65	-85	-92	47	141
Molecular → Tensor	-10	75	60	83	89	89
Frame	91	-132	56	111	-89	89

[a]The range of satisfactory simulations was found by simultaneously varying the spin population on oxygen (0.15 ± 0.03) and copper (0.68 ∓ 0.03). Error in the dipolar coupling was taken from the range of hyperfine coupling calculated when the spin population was varied.

[b]Error was estimated by individually varying the principal values of the hyperfine coupling until fits were visually unsatisfactory.

1.d: Comparison of experimental EPR results to DFT EPR property calculations

Table S1E: Results from DFT EPR property calculations[a] (hyperfine and quadrupole coupling in MHz).

g		Cu	H_S	H_R	N_{1basal}	N_{2basal}	F1	F2	F3
	Hyperfine								
2.076	xx	-6.65	38.10	30.26	30.92	31.42	-0.9	0.03	-0.57
2.115	yy	18.10	39.52	31.78	31.92	32.46	1.52	-0.91	1.27
2.237	zz	-688.29	46.44	38.64	40.26	40.91	-1.67	-1.74	-1.91
	Quadrupole								
	xx				-0.7441	-0.7538			
	yy				-1.0109	-1.0012			
	zz				1.7550	1.7550			

[a] ORCA, unrestricted Kohn-Sham theory, B3LYP functional, EPR-II basis set, specialized CP(PPP) basis set on copper for improved capture of core polarization.

Table S1F: Comparison of experimental[a] and calculated[b] spin populations

	Cu	O (error)	H_R	H_S	N_{1basal}	N_{2basal}
Experimental spin population	0.73 (0.03)	0.10 (0.03)	0.018	0.006	0.09	0.05
Mulliken spin population	0.597	0.230	0.016	0.019	0.0764	0.0786

[a] Spin population determined from single-crystal ^{1}H ENDOR using the distributed point dipole approximation.

[b] ORCA, unrestricted Kohn-Sham theory, B3LYP functional, EPR-II basis set, specialized CP(PPP) basis set on copper for improved capture of core polarization

1.e: Visualization of laboratory, crystal, molecular and tensor frames

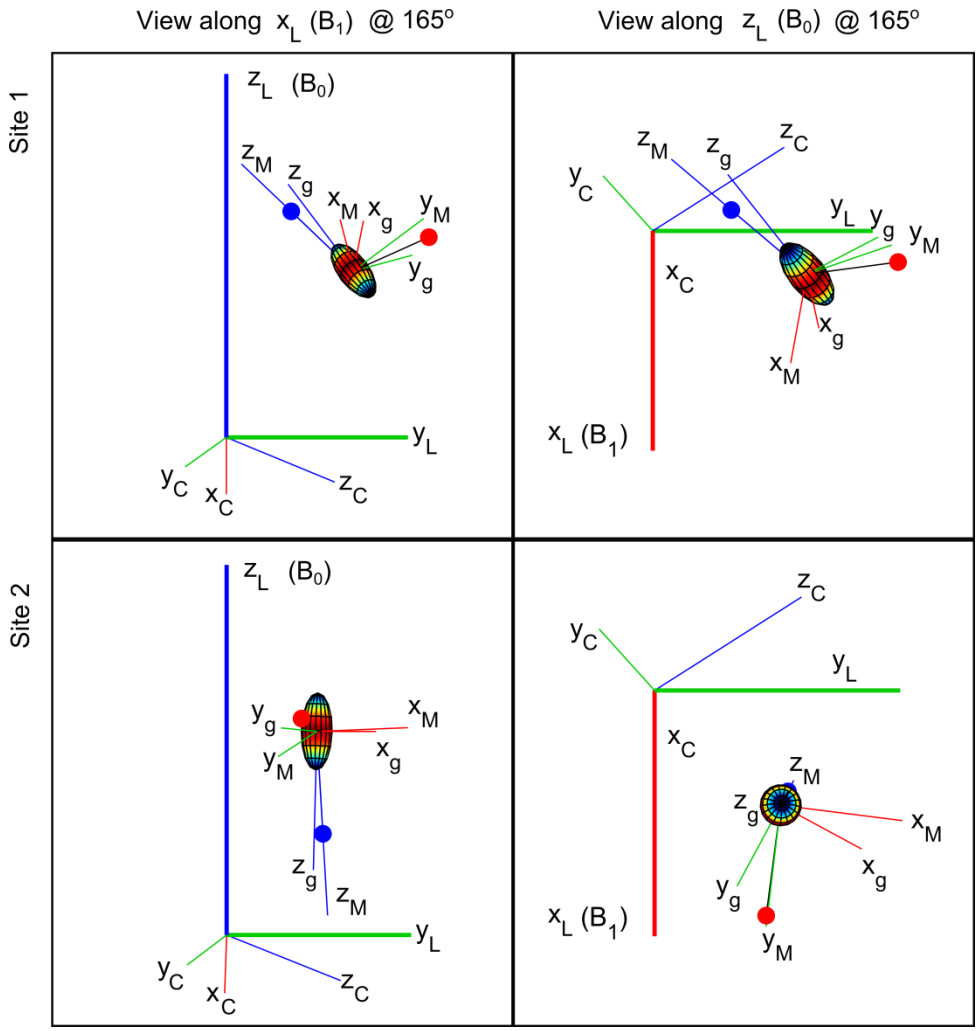

Figure S6A. The orientation of Cu^{II}-O(TFE) in the laboratory frame for crystal 1 (Figure 2C and Figure 4) at the 165° rotation increment. There are two EPR active sites in the crystal due to the $P2_1/n$ space group of the crystal. Site 2 is highlighted by a dotted line in Figure 2C. The axial nitrogen ligand (blue dot) and the oxygen of the trifluoroethoxide ligand (red dot) are labeled. The ellipsoid represents the g tensor and is centered on the copper nucleus. The subscripts L, C, M, and g stand for laboratory, crystal, molecular and g tensor, respectively. In all cases x axes are shown in red, y axes in green, and z axes in blue. The crystal was rotated around the y_L axis.

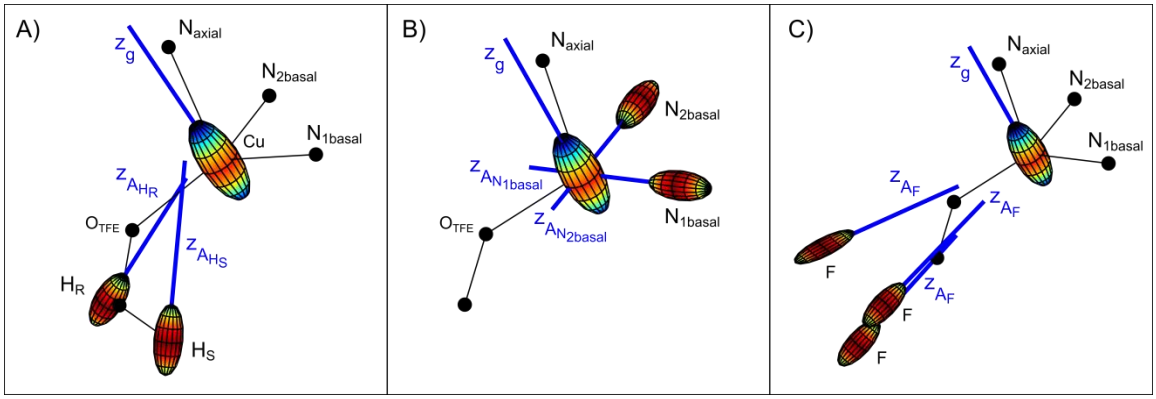

Figure S6B. Illustrated direction of the principle *z* component (blue, thick line) of the hyperfine tensors and *g* tensor in Cu^{II}-O(TFE). In all cases, an axial *g* tensor ellipsoid is centered on copper and ligand atoms are represented by black dots and the bonds by thin black lines. A) Hyperfine tensor ellipsoids for the hydrogen atoms of the trifluoroethoxide ligand are shown. Frames are generated by extracting the rotation matrix from the diagonalized hyperfine tensor calculated from the point dipole approximation. For these frames, the hyperfine tensor was calculated using an isotropic *g* value to remove contributions from the interaction between the hydrogen nucleus and the spin orbital. B) Hyperfine tensor ellipsoids for basal nitrogen nuclei of the Tp^{tBu} ligand. These frames were defined so that the largest principal value of the hyperfine coupling points towards copper, as described in the Experimental section of the main text. C) Hyperfine tensor ellipsoids for fluorine nuclei of the trifluoroethoxide ligand. These frames were defined so that the largest principal value of the hyperfine coupling points towards copper, as described in the Experimental section of the main text.

1.f: Derivation of nitrogen spin density from ^{14}N ENDOR following Morton and Preston[1]

Isotropic: The isotropic hyperfine coupling can be computed using the equation $\frac{8\pi}{3} g_e \mu_B g_N \mu_N \Psi^2(0)$ where $\Psi^2(0)$ represents the spin population in an s orbital. For nitrogen, the above yields a hyperfine coupling of 1811 MHz when 100% of the spin density is in the 2s orbital. Using the experimental isotropic hyperfine values of 32.9 and 31.8 MHz, we can compute the spin density $\rho(2s)$ using the simple relation

$$N_1 \qquad \rho(2s) = 100 \times \frac{32.9}{1811} = 1.81\ \%$$

$$N_2 \qquad \rho(2s) = 100 \times \frac{31.9}{1811} = 1.76\ \%$$

Anisotropic: The anisotropic component of the hyperfine coupling is a traceless tensor with principle values [2b –b –b] where b can be computed from the hyperfine values. For N_{1basal}, $b_{N1} = \frac{1}{3}(a_{\parallel} - a_{\perp}) = 4.1$ MHz and for N_{2basal}, $b_{N2} = \frac{1}{3}(a_{\parallel} - a_{\perp}) = 1.6$ MHz, assuming the hyperfine values have same sign. The anisotropic (dipolar) hyperfine coupling in a p, d, or f orbital can be computed using the equation $\alpha g_e \mu_B g_N \mu_N \langle r^{-3} \rangle$. Here, $\alpha = \frac{2}{5}$ for a p orbital and $\langle r^{-3} \rangle$ is obtained from the Hartree-Fock-Slater orbitals. For nitrogen, the resulting hyperfine coupling will be 55.5 MHz when 100% of the spin density is in a 2p orbital. We can compute the spin density $\rho(2p)$ using the simple relation

$$N_1 \qquad \rho(2p) = 100 \times \frac{4.1}{55.52} = 7.38\ \%$$

$$N_2 \qquad \rho(2p) = 100 \times \frac{1.6}{55.52} = 2.88\ \%$$

The final results are ≈ 9 % spin density on N_{1basal} and ≈ 5 % spin density on N_{2basal}.

1.g: 3 Pulse ESEEM

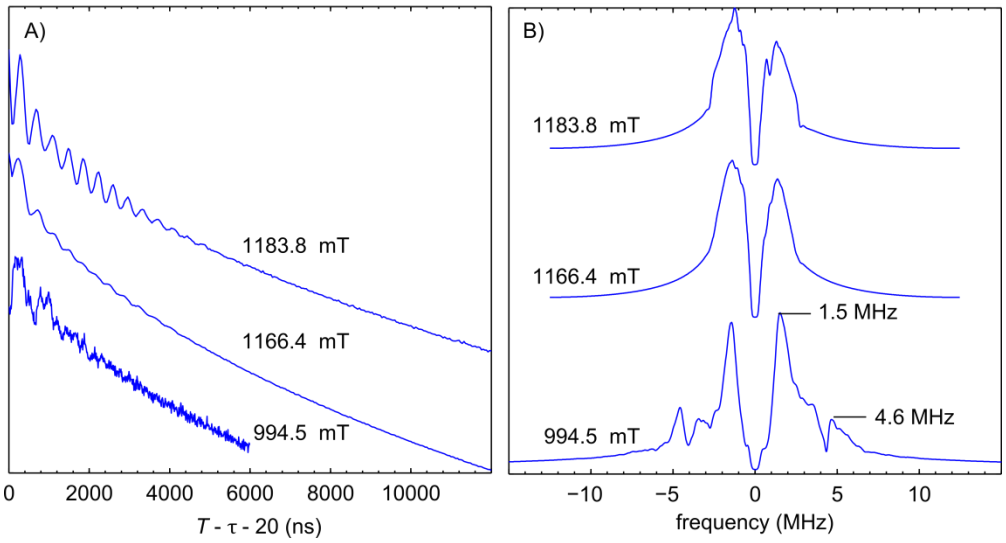

Figure S7. Orientation selection in 3 pulse electron spin echo envelope modulation (ESEEM) experiments recorded at field values listed in the figure on ≈ 1.5 mM Cu^{II}-O(TFE) in 1:1 DCM:toluene. A) At 1166.4 mT and 1183.8 mT, spectra were echo-detected [$\pi/2$(60 ns) – τ(180 ns) – $\pi/2$(60 ns) – T(200ns + t) – $\pi/2$(60 ns) – echo] at 34.081 GHz (10 K, 3 ms repetition time) with an increment in T of t = 40 ns. At 994.5 mT, spectra were echo-detected [$\pi/2$(60 ns) – τ(160 ns) – $\pi/2$(60 ns) – T(180ns + t) – $\pi/2$(60 ns) – echo] at 34.081 GHz (10 K, 3 ms repetition time) with an increment in T of t = 10 ns. B) Fourier transforms of the ESEEM spectra in A) show only very small (< 3 MHz) modulation frequencies at 1166.4 mT and 1183.8 mT. At 994.5 mT, frequencies of 1.5 MHz and 4.5 MHz are observed. The expected Larmor frequency of ^{14}N at this field is 3.05 MHz so this may correspond to the A_{zz} component of the axial nitrogen hyperfine coupling. However, isotopic labeling is needed to confirm this assignment.

Section 2: Supplemental electronic absorption and MCD spectra

2.a: Temperature dependence of MCD signal

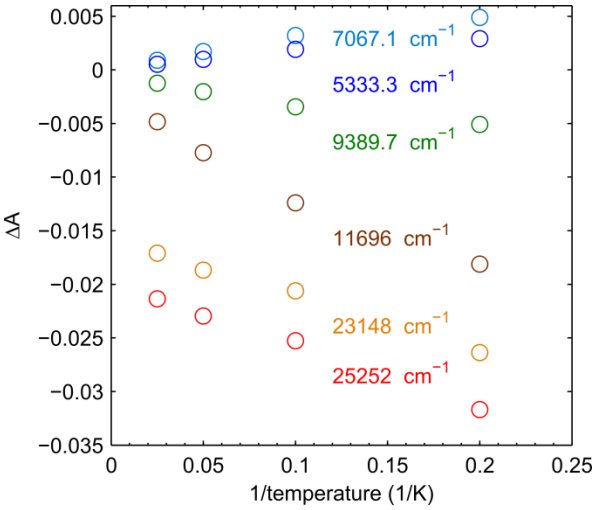

Figure S8: Temperature dependence of MCD absorption maxima for positive features and minima for negative features taken at 6 T and varying temperature. There is no significant saturation of the signal at 5 K, meaning the peak maxima of this spectrum can be used in the C_0/D_0 comparison discussed in the main text.

2.b: Full UV-Vis absorption spectrum

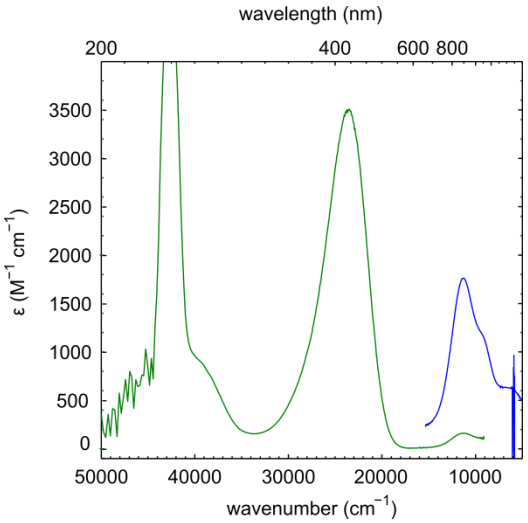

Figure S9: Room temperature UV-Vis and near-IR absorbtion spectra. The high energy transitions near 40000 cm^{-1} prevent the pseudo-σ transition (near 26000 cm^{-1}) from returning to a zero baseline at wavelengths shorter than 360 nm. In addition, the light source for the MCD spectrometer did not go to wavelengths shorter than 380 nm so the full transition could not be included in the Gaussian fit discussed in the main text. As such, the room temperature absorption spectrum was truncated at ~ 310 nm for fitting.

2.c: Electronic absorption and MCD fitting parameters

Table S2: Gaussian resolved fitting parameters for MCD, 5 K absorption, and room temperature absorption

Peak	Donor to Cu $d_{x^2-y^2}$	λ_{max} (cm^{-1})	integrated area	Full Width at Half Maximum (cm^{-1})	Maximum (ΔA, ε)	ΔA (MCD) / ε (RT ABS)[a] ($\times 10^3$)	f_{exp} [b]
1 MCD	d_{z^2}	5185	3	1033	0.0025	0.076	
LT ABS			N.A.	N.A.	N.A.		
RT ABS			1×10^5	4006	33		6.1×10^{-4}
2 MCD	d_{xy}	7047	10	1967	0.0048	0.16	
LT ABS			N.A.	N.A.	N.A.		
RT ABS			1×10^5	2440	30		3.4×10^{-4}
3 MCD	d_{yz+xz}	9403	-4	787	-0.0049	-0.053	
LT ABS			N.A.	N.A.	N.A.		
RT ABS			2×10^5	2290	93		9.8×10^{-4}
4 MCD	d_{yz-xz}	11807	-33	1726	-0.018	-0.12	
LT ABS			N.A.	N.A.	N.A.		
RT ABS			4×10^5	2400	157		0.0017
5 MCD	O(TFE) p_{π}	23205	-81	3121	-0.024	-0.0090	
LT ABS			1027	3377	N.A.		
RT ABS			118×10^5	4065	2722		0.0510
6 MCD	O(TFE) $p_{\sim\sigma}$	26066	-97	3210	-0.028	-0.021	
LT ABS			889	3282	N.A.		
RT ABS			87×10^5	6073	1340		0.0375

Fitting parameters are reported here with more significant figures than reported in the main article and are the result of the least-squares fitting described in the main text. Significant figures in the main article are based on the 2 nm step size used to record the MCD near-UV data (equivalent to a < 200 cm^{-1} step size) and the 5 nm step size used to record the MCD near-IR data (equivalent to a < 100 cm^{-1} step size for bands 3 and 4 and < 50 cm^{-1} step size for bands 1 and 2).

[a] $\Delta A/\varepsilon$ is an approximation of the commonly used C_0/D_0 ratio to compare the expected increase in intensity of transitions centered on nuclei with large spin orbit coupling in an MCD spectrum.

[b] The experimental oscillator strength is calculated as $f_{\text{exp}} = 4.61 \times 10^{-9} \epsilon_{\max} \nu_{1/2}$ using the $\epsilon_{\max}$ and the full width at half maximum $\nu_{1/2}$ of the transitions in the RT ABS spectrum.

2.d: Alternative interpretation of near-IR transitions in MCD spectrum

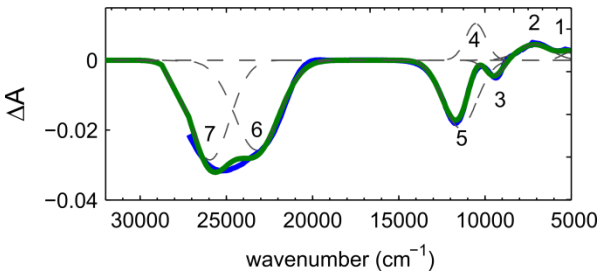

Figure S10. MCD spectrum acquired at 5 K and 6 T. Individual Gaussian resolved bands are shown as dashed gray lines, the total fit in green, and experimental data in blue. In the near IR region, 5 Gaussian transitions are used in the fit. Although these d → d transitions have the expected sign based on previous literature data, this analysis is not preferred. In this analysis, the $d_{xy} \rightarrow d_{x^2-y^2}$ transition energy is 9534 cm^{-1}. This is much larger than the small transition energy necessary to drive the large g_{zz} shift.

Table S3: Gaussian resolved fitting parameters for 5K, 6T MCD spectrum using five peaks in the near-IR region

Peak	Donor to Cu $d_{x^2-y^2}$	λ_{max} (cm^{-1})	integrated area	Full Width at Half Maximum (cm^{-1})	Maximum (ΔA)
1	d_{z^2}	5060	3	1219	0.0022
2	N(Py)	7116	11	2287	0.0045
3	d_{xy}	9534	-6	1280	-0.0044
4	d_{yz+xz}	10538	15	1376	0.0105
5	d_{yz-xz}	11450	-47	2284	-0.0193
6	O(TFE) p_π	23226	84	3059	-0.0257
7	O(TFE) p_σ	25950	81	2674	-0.0286

Section 3: Supplemental results of resonance Raman and Raman calculations

3.a: Tabulated experimental and calculated resonance Raman results

Table S4A: Experimental and calculated resonance Raman shifts and their shifts upon isotopic labeling

Mode [a]	Experimental Raman shift [b] (cm^{-1})	Isotopic shift, ^1H-^2H (cm^{-1})	Calculated Raman shift [c] (cm^{-1})	Calculated isotopic shift, ^1H-^2H (cm^{-1})
ν(Cu-O) + δ(F-$C_β$-F)	524	-3	497	-1
	521		496	
ν(Cu-O)	592	-25	553	-20
	567		533	
ν(Cu-O) + δ(O-C-$C_β$)	690	-12	663	-13
	678		650	
ν(C-O)	1139	+15	1094	+30.4
ν(C-O) + w(C-D)	1154[d]		1125	
ν(C-O)	1139	+15	1094	-8
ν(C-O) + ν($C_β$-F)	1154[d]		1086	
w(C-H)	1274	-266	1353	-389
	1008		964	
ν(C-$C_β$) + w(C-H)	1274	-266	1215	-251
w(C-D)	1008		964	

[a] Experimental modes are assigned based on the DFT calculation after visualizing normal modes in Avogadro. All motions describe the copper atom or the trifluoroethoxide ligand. When not specified, C corresponds to the α carbon. In some cases, modes on the trifluoroethoxide ligand change upon deuteration and the dominant motions are listed for Cu^{II}-O(TFE) (top) and Cu^{II}-O(TFE)-d_2 (bottom) in the split cells.

[b] The split cells for each mode list the resonantly enhanced Raman shift for Cu^{II}-O(TFE) (top) and the Raman shift for Cu^{II}-O(TFE)-d_2 (bottom).

[c] The split cells for each mode list the calculated resonantly enhanced Raman shift for Cu^{II}-O(TFE) (top) and the calculated Raman shift for Cu^{II}-O(TFE)-d_2 (bottom).

[d] This peak lays underneath a DCM solvent peak and cannot be confirmed as peaks due to the sample Cu^{II}-O(TFE)-d_2 as discussed in the main text.

3.b: Sample input file for resonance Raman calculations

```
! UKS B3LYP tzvp tzvp/j RIJCOSX PAL6
! MORead TightSCF NMGrad Grid5
%maxcore 4000
%moinp "Cu_opt.gbw"
%tddft
       MaxDim 52
       nRoots 13
end
%rr     States 10,12
       HessName "Cu_AnFreq.hess"
       ASAInput true
       end
*xyzfile 0 2 Cu_opt.xyz
```

3.c: Raman calculation in Orca 3.0.3

The calculation of ground state vibrational frequencies and normal mode polarizabilities was performed with numerical differentiation with an increment of 0.005 a_0. An identical level of theory as for the geometry optimization was used but included the resolution of the identity (RI) approximation with the auxiliary tzvp/j basis set.[2–4] The SCF was reconverged with the new basis set and a convergence criterion of $1x10^{-8}$ E_h. Vibrational frequencies for isotope shifts upon deuteration of the trifluoroethoxide ligand were calculated using the standalone orca_vib program. The hessian output file of the ground state frequency calculation was used as input to orca_vib after manually modifying the masses of the appropriate hydrogen atoms. A grid size of 4 correctly modelled the number of electrons for the system as necessary for accurate results for vibrational frequencies. In both frequency calculations, no negative frequencies were observed suggesting the calculations are reliable and run from an energy minimum.

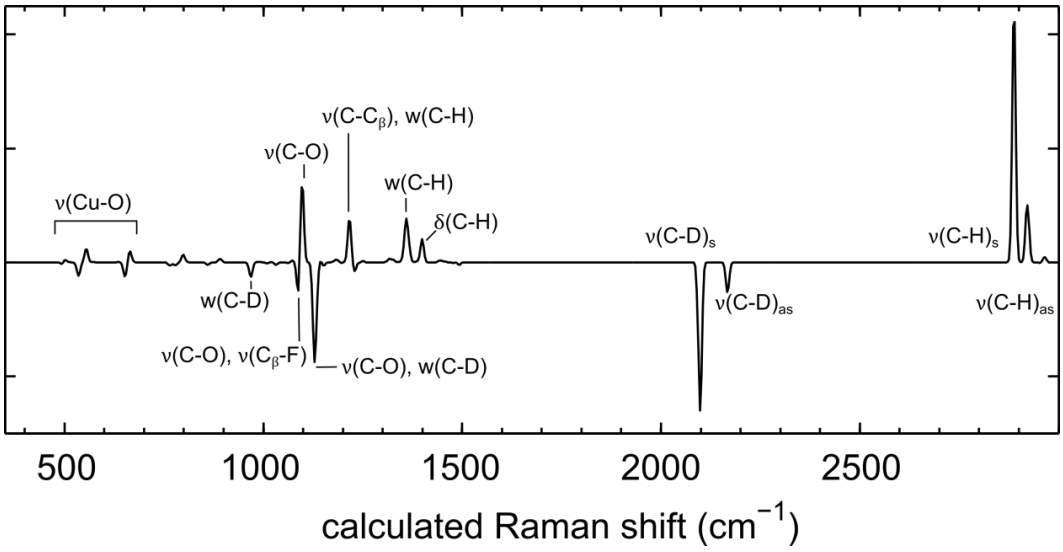

Figure S11. Difference spectrum (Cu^{II}-O(TFE) − Cu^{II}-O(TFE)-d_2) of predicted Raman enhancement of vibrational modes. Peaks due to Cu^{II}-O(TFE) appear as positive features, and peaks due to Cu^{II}-O(TFE)-d_2 appear as negative features. Notably, for Cu^{II}-O(TFE), a ν(C-C_β) + w(C-H) mode at 1216.7 cm^{-1} and a w(C-H) mode at 1359.2 cm^{-1} are predicted to have Raman activity. However, neither of these modes are predicted to have resonance enhancement.

Table S4B: Calculated Raman shifts and shifts upon isotopic labeling

Normal Mode	Cu^{II}-O(TFE) Raman shift (cm^{-1})	Normal Mode	Cu^{II}-O(TFE)-d_2 Raman shift (cm^{-1})	Isotopic shift (cm^{-1})
ν(Cu-O) + δ(F-C_β-F)	498	ν(Cu-O) + δ(F-C_β-F)	497	-1
ν(Cu-O)	555	ν(Cu-O)	535	-20
ν(Cu-O) + δ(O-C-C_β)	664	ν(Cu-O) + δ(O-C-C_β)	652	-12
ν(C-O)	1097	ν(C-O) + w(C-D)	1128	31
ν(C-O)	1097	ν(C-O) + ν(C_β-F)	1090	-7
w(C-H)	1359	w(C-D)	968	-391
ν(C-C_β) + w(C-H)	1217	w(C-D)	968	-249
δ(C-H)	1400			
ν(C-H)s	2888	ν(C-D)s	2098	-790
ν(C-H)as	2921	ν(C-D)as	2167	-754

Section 4: Structural and spectroscopic properties of Cu^{II} complexes

Table S5: Structural comparison of Cu^{II}-alkoxide, Cu^{II}-alkylperoxo,[5] and Cu^{II}-thiolate[6]

Structural feature [a]	Cu-OR	Cu-OOR[b]	Cu-SR[c]
Cu-N_{axial}	2.227	2.16	2.119
Cu-LMCT donor	1.832	1.81	2.176
Cu-N_{1basal}	1.972	1.96	1.930
Cu-N_{2basal}	1.964	1.98	2.037
OC,OO,SC	1.359	1.46	
Cu-X-X angle	135.48	112.1	111.7
Cu-X-X-C dihedral	158.19	179.3	
Nax-Cu-X	104.96		112.7

[a] Units are Ångstroms for bond lengths and degrees for angles.

[b] $Cu(OOCMe_2Ph)(HB(3,5\text{-}^{i}Pr_2Pz)_3)$

[c] $Cu(SC_6F_5)(HB(3,5\text{-}^{i}Pr_2Pz)_3)$

Table S6: Spectroscopic comparison of Cu^{II}-alkoxide, Cu^{II}-alkylperoxo,[7] and Cu^{II}-thiolate[8]

	Cu-OR	Cu-OOR[a]	Cu-SR[b]
g_{zz}	2.45	2.316	2.21
$g_{\perp}$ (X-band)	2.079	2.097	
$^{Cu}A_{zz}$ ($\times 10^4$ cm^{-1})	-40	-55	-72
$E_{x^2-y^2} - E_{xy}$(cm^{-1})	7047	8050	9250
f, oscillator strength $p_{\sim\sigma}$ CT donor → Cu $d_{x^2-y^2}$	0.0375	0.009	0.0002
f, oscillator strength p_{π} CT donor → Cu $d_{x^2-y^2}$	0.0510	0.056	0.0713

[a] $Cu(OOCMe_2Ph)(HB(3,5\text{-}^{i}Pr_2Pz)_3)$, where $-OOCMe_2Ph$ is the CT donor to Cu $d_{x^2-y^2}$

[b] $Cu(SCPh_3)(HB(3,5\text{-}^{i}Pr_2Pz)_3)$, where $-SCPh_3$ is the CT donor to Cu $d_{x^2-y^2}$

Section 5: Additional calculation results and details

5.a: Time-dependent DFT

A time-dependent DFT calculation was used to produce the UV-Vis spectrum and the difference density maps of the transitions shown in Figure S11. In these figures, the grey surface represents the acceptor state and the purple the donor state. In the near IR region, the first four calculated transitions (1-4) show substantial copper d orbital character in the donor state and are assigned as dominantly d_{z^2}, $d_{xz/yz}$, d_{xy}, and $d_{xz/yz}$ in character, respectively. The expected order of the transition donors (lowest to highest transition energy) in a distorted tetrahedral environment is d_{z^2}, d_{xy}, $d_{xz/yz}$, and $d_{xz/yz}$.[7,8] These have been assigned based on MCD experiments and typically show a + − + − sign pattern, respectively. Based on the sign of the transitions in this work, transitions 1-4 in the experimental MCD spectrum could be assigned as (+)d_{z^2}, (+)$d_{xz/yz}$, (−)d_{xy}, and (−)$d_{xz/yz}$, respectively, which matches the order of the TDDFT calculation but does not match the order of the d manifold transitions based on the literature. This order also does not support the difference in energy $E_{x^2-y^2} - E_{xy}$ necessary to drive the large g_{zz}.

The charge transfer transitions from the ethoxide ligand are calculated to be in the near-UV region as seen experimentally. In the calculation, the O(TFE) $p_{\sim\sigma}$ transition (labeled 5) is lower in energy and less intense than the O(TFE) p_{π} transition (labeled 6). The lower intensity is due to poor overlap of the O(TFE) $p_{\sim\sigma}$ orbital with the acceptor Cu $d_{x^2-y^2}$. It is unexpected that the O(TFE) $p_{\sim\sigma} \rightarrow$ Cu $d_{x^2-y^2}$ transition is lower in energy in the calculation as this orbital is stabilized (larger transition energy) due to the σ bonding interaction it has with copper.

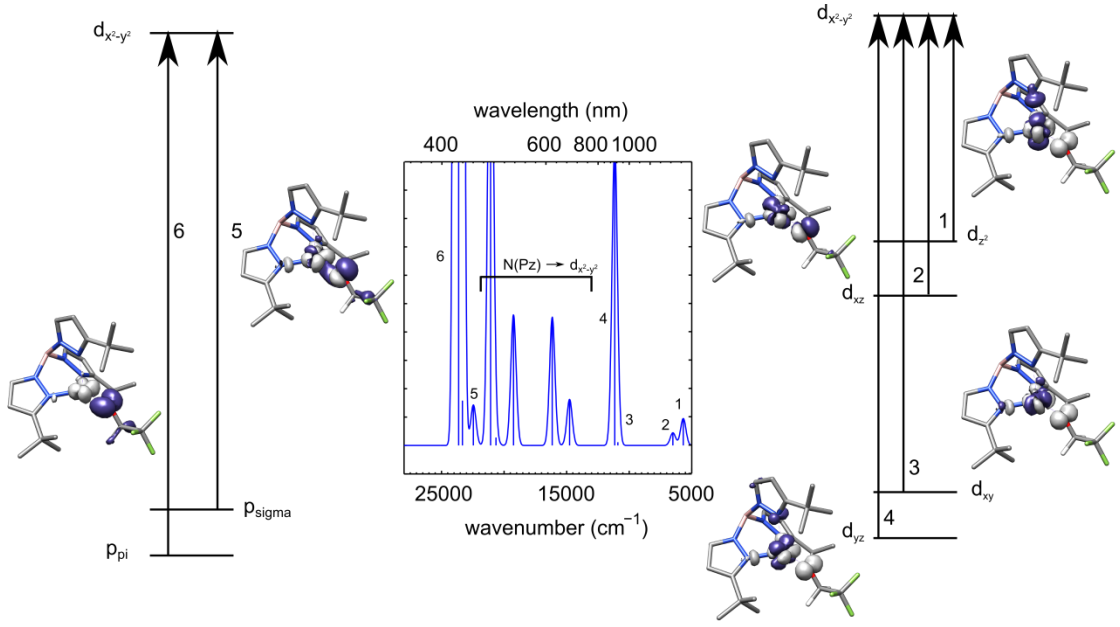

Figure S12. Calculated absorption spectrum and difference density plots. Grey represents the acceptor state and purple the donor state.

5.b: Comparison of crystal structure geometry and optimized geometry

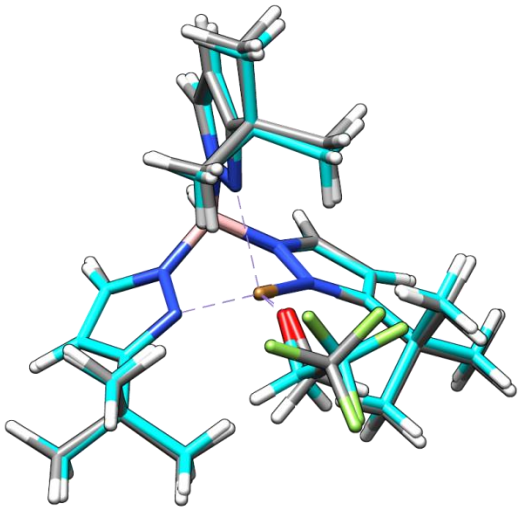

Figure S13. Comparison of XYZ coordinates of crystal structure (cyan) and optimized geometry (grey) of Cu^{II}-O(TFE).

Table S7: Structural comparison of crystallographic and calculated geometry of Cu^{II}-O(TFE)

Structural feature [a]	Crystal	Calculated
Cu-N_{axial}	2.227	2.26
Cu-O	1.832	1.87
Cu-N_{1basal}	1.972	2.01
Cu-N_{2basal}	1.964	2.01
O-C	1.359	1.38
Cu-O-C	135.48	134.006
Nax-Cu-O	104.96	105.307
Cu-O-C-C	158.19	-177.771
Cu-O-C-H_R	-81.06	-57.700
Cu-O-C-H_S	37.43	62.855

[a] Units are Ångstroms for bond lengths and degrees for angles.

Optimized geometry (UKS BP86 TZVP) in *xyz* coordinates

Used for EPR property calculations, frequency, and time-dependent DFT calculations

C	-1.29092	3.41700	-3.90409
C	-1.17568	0.94198	-3.50157
C	-0.75923	2.32666	-2.95423
C	0.780537	2.428944	-2.889226
C	2.002332	-2.543908	-2.875725
C	1.902269	-1.191829	-2.159336
C	-1.33992	2.52492	-1.56372
C	-2.27253	3.49019	-1.13019
C	-2.06995	-3.01677	-1.13184
C	-2.46720	3.24476	0.22399
C	3.590114	1.263303	0.189568
C	-1.89501	-3.28576	0.37974
C	-0.44591	-3.73826	0.66676
C	-2.85901	-4.41358	0.79844
C	-2.20637	-2.02243	1.16850
C	3.367469	-0.926622	1.443219
C	3.394876	0.613414	1.577575
C	2.089793	1.099865	2.184496
C	-3.20815	-1.84534	2.15172
C	4.577313	1.012647	2.480703
C	-3.09054	-0.52813	2.56715
C	1.882996	1.757323	3.414894
C	0.515358	1.993563	3.490081
H	-0.86127	3.27542	-4.90659
H	-0.77198	0.79697	-4.51557
H	-2.38571	3.36842	-4.00048
H	1.217227	2.273047	-3.887511
H	-2.27090	0.85665	-3.55488
H	-1.01594	4.42505	-3.55975
H	1.810332	-0.422295	-2.952385
H	-0.80631	0.12625	-2.86469
H	1.097728	3.417018	-2.524609
H	1.196175	1.672204	-2.207509
H	2.883458	-1.028027	-1.669107
H	-1.88553	-3.93968	-1.70352
H	-2.73913	4.26693	-1.72443
H	-1.35828	-2.25767	-1.47968
H	-3.09172	-2.67297	-1.35312
H	2.757876	1.013051	-0.484903
H	4.526478	0.910148	-0.268536
H	-0.23015	-4.67565	0.13101
H	-2.63322	-5.32226	0.22082
H	0.275396	-2.983645	0.328649
H	3.637085	2.359221	0.270525
H	-3.90828	-4.14497	0.60305
H	-3.09670	3.73783	0.95767
H	2.527260	-1.263806	0.820468
H	4.303124	-1.282178	0.984370
H	-0.29756	-3.91571	1.74279
H	-2.75669	-4.66082	1.86613
H	5.517987	0.656134	2.035452
H	3.267946	-1.404576	2.428841
H	-3.92055	-2.57889	2.51044
H	4.650464	2.104527	2.593669
H	-2.20471	2.10463	2.78425
H	-3.64811	0.04465	3.30176
H	4.491383	0.564041	3.481382
H	2.632160	2.028837	4.149319

H	-0.08775	2.47142	4.25528
B	-1.56434	1.49282	1.96397
N	-1.00486	1.74233	-0.50824
N	-1.69649	2.19287	0.58048
N	-1.52075	-0.86561	1.00414
N	0.892735	0.950875	1.565356
N	-2.07588	0.04200	1.86964
N	-0.06260	1.50492	2.36984
O	0.853543	-1.159658	-1.256910
F	3.056084	-2.523999	-3.752006
F	0.885020	-2.835728	-3.592992
F	2.213090	-3.573094	-2.013744
Cu	0.155360	0.151314	-0.126235

xyz coordinates from crystal structure .cif file

C	-1.19804	3.41553	-3.86799
C	-1.23501	0.93749	-3.50294
C	-0.74824	2.28779	-2.93958
C	0.78459	2.30614	-2.87083
C	2.14904	-2.48764	-2.56264
C	1.67785	-1.08437	-2.30589
C	-1.33505	2.50317	-1.56265
C	-2.27388	3.45856	-1.14895
C	-2.10338	-2.86728	-1.14005
C	-2.47558	3.21905	0.19249
C	3.52894	1.15998	0.19333
C	-1.82030	-3.20578	0.33253
C	-0.34906	-3.61722	0.48644
C	-2.71448	-4.37415	0.76562
C	-2.12169	-1.98916	1.18159
C	3.20224	-1.00418	1.44240
C	3.31369	0.52216	1.57239
C	2.04613	1.07489	2.18087
C	-3.08021	-1.85689	2.19784
C	4.51932	0.87231	2.45184
C	-2.99414	-0.54981	2.61399
C	1.86135	1.74474	3.39207
C	0.51150	2.03343	3.45935
H	-0.76245	3.31432	-4.73987
H	-0.84003	0.79128	-4.38787
H	-2.17064	3.37636	-3.98220
H	1.15360	2.13433	-3.76222
H	-2.21202	0.94851	-3.57900
H	-0.94957	4.27920	-3.47699
H	1.25868	-0.71988	-3.12530
H	-0.96244	0.21468	-2.89994
H	1.08690	3.18336	-2.55551
H	1.09205	1.61234	-2.25078
H	2.45135	-0.51143	-2.07470
H	-1.88505	-3.64068	-1.70080
H	-2.68439	4.12963	-1.68147
H	-1.55438	-2.10197	-1.41064
H	-3.05143	-2.64335	-1.24733
H	2.76634	0.95157	-0.38565
H	4.34965	0.80392	-0.20677
H	-0.15748	-4.37313	-0.10707
H	-2.51459	-5.16001	0.21528
H	0.22813	-2.86152	0.24960
H	3.60854	2.13186	0.29155
H	-3.65548	-4.12547	0.65045
H	-3.06029	3.70781	0.75971
H	2.42849	-1.22881	0.88443

H	4.01717	-1.35696	1.02796
H	-0.17880	-3.87971	1.41509
H	-2.54491	-4.58350	1.70785
H	5.33961	0.54680	2.02598
H	3.08986	-1.40045	2.33149
H	-3.66482	-2.52874	2.52838
H	4.57191	1.84475	2.56169
H	-2.11860	2.03655	2.63080
H	-3.51939	-0.14806	3.29607
H	4.41694	0.44937	3.32979
H	2.52594	1.95803	4.03638
H	0.07657	2.48931	4.17040
B	-1.57424	1.53456	1.95859
N	-1.00113	1.73377	-0.51303
N	-1.71321	2.18551	0.56497
N	-1.48503	-0.81465	1.00171
N	0.85407	0.96774	1.55677
N	-2.03577	0.06675	1.88817
N	-0.08170	1.56149	2.35209
O	0.77771	-1.06769	-1.28749
F	3.03777	-2.50838	-3.57824
F	1.15311	-3.32337	-2.88762
F	2.76174	-3.02755	-1.50780
Cu	0.16109	0.19305	-0.10931

Section 6: Synthesis and crystallographic information for $Tp^{tBu}Zn^{II}(OCH_2CF_3)$

6.a: Unit cell dimensions compared to $Tp^{tBu}Cu^{II}(OCH_2CF_3)$[9]

$Tp^{tBu}Cu^{II}(OCH_2CF_3)$		$Tp^{tBu}Zn^{II}(OCH_2CF_3)$	
a = 9.6749(12) Å	α = 90°	a = 9.5516(12) Å	α = 90°
b = 16.817(2) Å	β = 96.881(6)°	b = 17.010(2) Å	β = 95.412(7)°
c = 16.646(2) Å	γ = 90°	c = 16.615(2) Å	γ = 90°

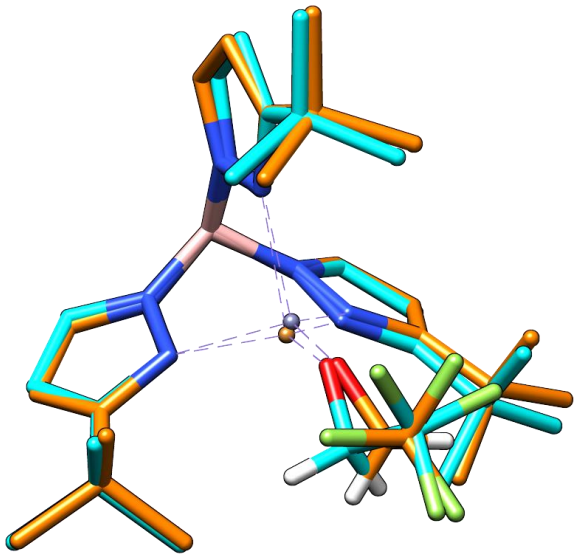

Figure S14. Visualization of the xyz coordinates of Cu^{II}-O(TFE) (carbon in cyan, copper in brown, nitrogen in blue, oxygen in red, fluorine in yellow) and Zn^{II}-O(TFE) (carbons in orange, zinc in purple, nitrogen in blue, oxygen in red, fluorine in yellow). Hydrogens are not shown for clarity, except on the trifluoroethoxide ligand (white). The xyz coordinates from the crystal structure files were related by a translation. This image was created using the match function in Chimera where the atoms C5,N3,N4,N1,C12,B1,C19 in Cu^{II}-O(TFE) were matched to the atoms C20, N4, N6, N3, C14, B1, C7 in Zn^{II}-O(TFE).

6.b: Synthesis and structural characterization of $Tp^{tBu}Zn^{II}$-OTf

General Considerations

Unless otherwise noted, all chemicals were purchased from Sigma-Aldrich and used without purification. Solvents were purchased from Fischer and dried using a "Grubbs type" Seca Solvent System installed by GlassContour. 2,2,2-trifluoroethanol was distilled from $CaSO_4$ with a small amount of $NaHCO_3$ and stored over 3Å molecular sieves. All glassware was dried in an oven at 150 °C overnight and pumped into a nitrogen filled glovebox while hot. Celite was dried at 100 °C overnight under vacuum. All reactions were performed in a nitrogen filled glovebox.

Preparation and Characterization of $Tp^{tBu}Zn^{II}$-OTf

hydro-*tris*(3-*tert*-butylpyrazol-1-yl)borate) zinc(II) triflate, $Tp^{tBu}Zn^{II}$-OTf:

To a toluene solution of 5 mL $Tp^{tBu}Zn^{II}Cl$ (328 mg, 0.68 mmol, prepared as previously described[10]) was added AgOTf (175 mg, 0.68 mmol) with stirring. A chalky gray-red precipitate formed over 1 hour and was collected by filtration on a Celite plug. Extraction with dichloromethane yielded a colorless solution, which upon removal of the solvent, gave $Tp^{tBu}Zn^{II}$-OTf as a white solid (367 mg, 91%). ^{1}H NMR (500 MHz, CD_2Cl_2): 7.62 (d, $^3J_{H\text{-}H}$ = 2.3 Hz, 3H), 6.12 (d, $^3J_{H\text{-}H}$ = 2.3 Hz, 3H), 1.37 (s, 27H). The product was crystallized from pentane at -30 °C yielding $Tp^{tBu}Zn^{II}$-OTf and a co-crystallized and disordered pentane molecule. Elemental Analysis was found to be slightly high in C and H which is likely a result of residual co-crystallized pentane. Anal. calcd. for $C_{22}H_{34}BF_3N_6O_3SZn$: C, 44.35; H, 5.75; N, 14.11. Found: C, 44.84; H, 5.91; N, 14.13.

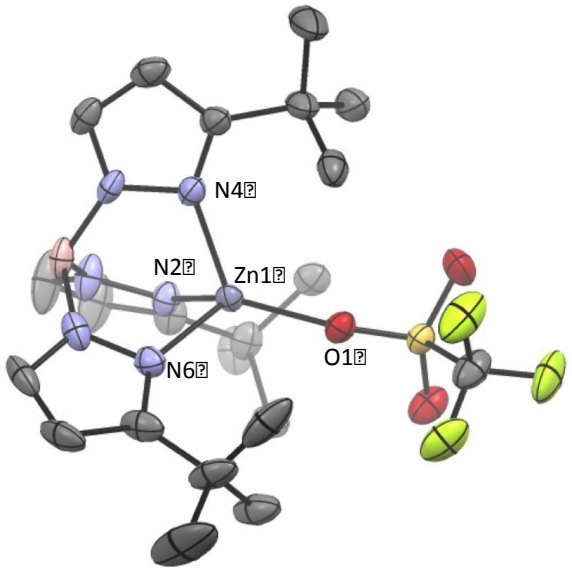

Figure S15. ORTEP drawing of $Tp^{tBu}Zn^{II}$-OTf with select atom labels showing 50% probability ellipsoids. Hydrogen atoms and the co-crystallized pentane molecule are omitted for clarity. Selected interatomic distances (Å) and angles (deg) are as follows: N2-Zn1, 2.010(4); N4-Zn1, 2.024(4); N6-Zn1, 2.018(4); O1-Zn1, 1.938(4); N2-Zn1-N4, 97.04(18); N2-Zn1-N6, 94.78(18); N2-Zn1-O1, 126.31(17); N4-Zn1-N6, 95.26(18); N4-Zn1-O1, 119.82(17); N6-Zn1-O1, 116.87(1).

Crystallographic Data for $Tp^{tBu}Zn^{II}$-OTf

General Procedure:

A colorless prism, measuring 0.30 × 0.20 × 0.05 mm^3 was mounted on a loop with oil. Data was collected at -173 ° C on a Bruker APEX II single crystal X-ray diffractometer, Mo-radiation.

Crystal-to-detector distance was 40 mm and exposure time was 10 seconds per frame for all sets. The scan width was 0.5°. Data collection was 99.1% complete to 25° in ϑ. A total of 93541 reflections were collected covering the indices, h = -12 to 12, k = -24 to 24, l = -18 to 18. 5986 reflections were symmetry independent and the R_{int} = 0.1165 indicated that the data was of slightly less than average quality (0.07). Indexing and unit cell refinement indicated a primitive monoclinic lattice. The space group was found to be P 2_1/n (No. 14).

The data was integrated and scaled using SAINT, SADABS within the APEX2 software package by Bruker.

Solution by direct methods (SHELXS, SIR97) produced a complete heavy atom phasing model consistent with the proposed structure. The structure was completed by difference Fourier synthesis with SHELXL97. Scattering factors are from Waasmair and Kirfel.[11] Hydrogen atoms were placed in geometrically idealized positions and constrained to ride on their parent atoms with C---H distances in the range 0.95-1.00 Å. Isotropic thermal parameters U_{eq} were fixed such that they were 1.2U_{eq} of their parent atom U_{eq} for CH's and 1.5U_{eq} of their parent atom U_{eq} in case of methyl groups. All non-hydrogen atoms were refined anisotropically by full-matrix least-squares.

The Zn complex is accompanied by a 4-fold disordered pentane.

Table S8: Crystallographic data for $Tp^{tBu}Zn^{II}$-OTf•Pentane provided.

Empirical formula	$C_{27}H_{46}BF_3N_6O_3SZn$
Formula weight	667.94
Temperature	100(2) K
Wavelength	0.71073 Å
Crystal system	Monoclinic
Space group	P21/n
Unit cell dimensions	a = 10.4203(10) Å α = 90°. b = 20.5076(19) Å β = 91.771(5)°. c = 15.4032(15) Å γ = 90°.
Volume	3290.0(5) $Å^3$
Z	4
Density (calculated)	1.348 Mg/m^3
Absorption coefficient	0.864 mm^{-1}
F(000)	1408
Crystal size	0.30 × 0.20 × 0.05 mm^3
Theta range for data collection	1.99 to 25.35°.
Index ranges	$-12 \le h \le 12$, $-24 \le k \le 24$, $-18 \le l \le 18$
Reflections collected	93541
Independent reflections	5986 [R(int) = 0.1165]
Completeness to theta = 25.00°	99.1 %
Max. and min. transmission	0.9581 and 0.7816
Refinement method	Full-matrix least-squares on F^2
Data / restraints / parameters	5986 / 11 / 380
Goodness-of-fit on F^2	1.140
Final R indices [I>2sigma(I)]	R1 = 0.0690, wR2 = 0.1576
R indices (all data)	R1 = 0.1007, wR2 = 0.1813
Largest diff. peak and hole	1.104 and -1.019 e.$Å^{-3}$

6.c: Synthesis and characterization of $Tp^{tBu}Zn^{II}$-OCH_2CF_3

hydro-*tris*(3-*tert*-butylpyrazol-1-yl)borate) zinc(II) 2,2,2-trifluoroethoxide, $Tp^{tBu}Zn^{II}$-OCH_2CF_3:

To a dichloromethane solution of 5 mL $Tp^{tBu}Zn^{II}$-OTf (363 mg, 0.61 mmol) was added a ~2 mL dichloromethane solution containing 1,8-Diazabicyclo[5.4.0]undec-7-ene (DBU; 93 mg, 0.61 mmol) and 2,2,2-trifluoroethanol (180 mg, 1.83 mmol). The reaction mixture was stirred for 30 minutes after which the solvent was removed in vacuo yielding a white solid (282 mg, 85%). ^{1}H NMR (500 MHz, CD_2Cl_2): 7.55 (d, $^3J_{H\text{-}H}$ = 2.3 Hz, 3H), 6.05 (d, $^3J_{H\text{-}H}$ = 2.3 Hz, 3H), 4.50 (q, $^3J_{H\text{-}F}$ = 9.5 Hz, 2H), 1.39 (s, 27H). $Tp^{tBu}Zn^{II}$-OCH_2CF_3 was extracted with ether and crystallized from pentane at -30 °C. Anal. calcd. for $C_{23}H_{36}BF_3N_6OZn$: C, 50.62; H, 6.65; N, 15.40. Found: C, 50.88; H, 6.80; N, 15.49.

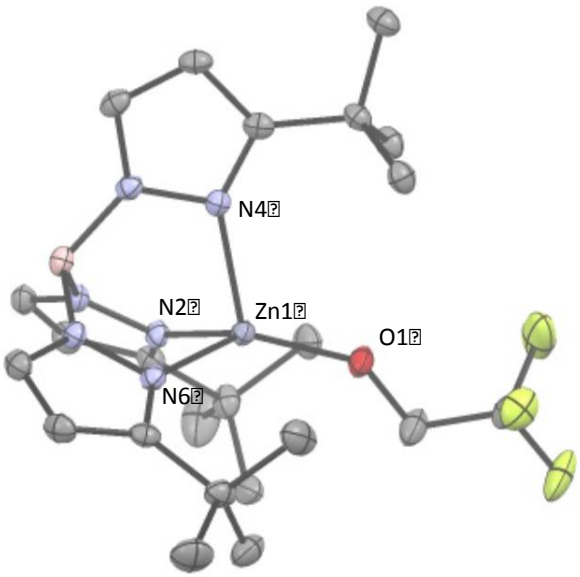

Figure S16. ORTEP drawing of $Tp^{tBu}Zn^{II}$-OCH_2CF_3 with select atom labels showing 50% probability ellipsoids. Hydrogen atoms are omitted for clarity. Selected interatomic distances (Å) and angles (deg) are as follows: N2-Zn1, 2.0304(16); N4-Zn1, 2.0586(16); N6-Zn1, 2.0553(16); O1-Zn1, 1.8471(14); N2-Zn1-N4, 92.64(6); N2-Zn1-N6, 94.71(6); N2-Zn1-O1, 129.59(7); N4-Zn1-N6, 93.51(6); N4-Zn1-O1, 113.76(6); N6-Zn1-O1, 123.63(7).

Crystallographic Data for $Tp^{tBu}Zn^{II}$-OCH_2CF_3

General Procedure:

A colorless prism, measuring 0.14 x 0.10 x 0.05 mm^3 was mounted on a loop with oil. Data was collected at -173°C on a Bruker APEX II single crystal X-ray diffractometer, Mo-radiation.

Crystal-to-detector distance was 40 mm and exposure time was 10 seconds per frame for all sets. The scan width was 0.5°. Data collection was 100% complete to 25° in ϑ. A total of 117542 reflections were collected covering the indices, h = -12 to 12, k = -22 to 22, l = -22 to 22. 6749 reflections were symmetry independent and the R_{int} = 0.0842 indicated that the data was of slightly less than average quality (0.07). Indexing and unit cell refinement indicated a primitive monoclinic lattice. The space group was found to be P 2_1/n (No.14).

The data was integrated and scaled using SAINT, SADABS within the APEX2 software package by Bruker.

Solution by direct methods (SHELXS, SIR97) produced a complete heavy atom phasing model consistent with the proposed structure. The structure was completed by difference Fourier synthesis with SHELXL97. Scattering factors are from Waasmair and Kirfel.[11] Hydrogen atoms were placed in geometrically idealised positions and constrained to ride on their parent atoms with C---H distances in the range 0.95-1.00 Å. Isotropic thermal parameters U_{eq} were fixed such that they were $1.2U_{eq}$ of their parent atom U_{eq} for CH's and $1.5U_{eq}$ of their parent atom U_{eq} in case of methyl groups. All non-hydrogen atoms were refined anisotropically by full-matrix least-squares.

Table S9: Crystallographic data for the structures provided.

Empirical formula	$C_{23}H_{36}BF_3N_6OZn$
Formula weight	545.76
Temperature	100(2) K
Wavelength	0.71073 Å
Crystal system	Monoclinic
Space group	P 2_1/n
Unit cell dimensions	
	a = 9.5516(12) Å α = 90°
	b = 17.010(2) Å β = 95.412(7)°
	c = 16.615(2) Å γ = 90°
Volume	2687.4(6) $Å^3$
Z	4
Density (calculated)	1.349 Mg/m^3
Absorption coefficient	0.961 mm^{-1}
F(000)	1144
Crystal size	0.14 × 0.10 × 0.05 mm^3
Theta range for data collection	1.72 to 28.55°.
Index ranges	$-12 \le h \le 12$, $-22 \le k \le 22$, $-22 \le l \le 22$
Reflections collected	117542
Independent reflections	6749 [R(int) = 0.0842]
Completeness to theta = 25.00°	100.0 %
Max. and min. transmission	0.9535 and 0.8772
Refinement method	Full-matrix least-squares on F^2
Data / restraints / parameters	6749 / 0 / 325
Goodness-of-fit on F^2	1.018
Final R indices [I>2sigma(I)]	R1 = 0.0346, wR2 = 0.0673
R indices (all data)	R1 = 0.0631, wR2 = 0.0781
Largest diff. peak and hole	0.325 and -0.397 $e.Å^{-3}$

References

(1) Morton, J. R.; Preston, K. F. *J. Magn. Reson.* **1978**, *30*, 577–582.
(2) Dunlap, B. I.; Connolly, J. W. D.; Sabin, J. R. *J. Chem. Phys.* **1979**, *71*, 3396–3402.
(3) Feyereisen, M.; Fitzgerald, G.; Komornicki, A. *Chem. Phys. Lett.* **1993**, *208*, 359–363.
(4) Neese, F.; Wennmohs, F.; Hansen, A.; Becker, U. *Chem. Phys.* **2009**, *356*, 98–109.
(5) Kitajima, N.; Katayama, T.; Fujisawa, K.; Iwata, Y.; Moro-oka, Y. *J. Am. Chem. Soc.* **1993**, *115*, 7872–7873.
(6) Kitajima, N.; Fujisawa, K.; Tanaka, M.; Moro-oka, Y. *J. Am. Chem. Soc.* **1992**, *114*, 9232–9233.
(7) Chen, P.; Fujisawa, K.; Solomon, E. I. *J. Am. Chem. Soc.* **2000**, *122*, 10177–10193.
(8) Randall, D. W.; George, S. D.; Hedman, B.; Hodgson, K. O.; Fujisawa, K.; Solomon, E. I. *J. Am. Chem. Soc.* **2000**, *122*, 11620–11631.
(9) (a) Porter, T. R. Ph. D. Thesis, University of Washington, Seattle, 2014.
(b) Porter, T. R.; Capitao, D.; Kaminsky, W.; Qian, Z.; Mayer, J. M.; **2016**, submitted manuscript
(10) Gorrell, I. B.; Looney, A.; Parkin, G. *J. Chem. Soc. Chem. Commun.* **1990**, *20*, 220–222.
(11) Waasmaier, D.; Kirfel, A. *Acta Crystallogr. Sect. A* **1995**, *51*, 416–431.